POLITECNICO
MILANO 1863

SCUOLA DI INGEGNERIA INDUSTRIALE
E DELL'INFORMAZIONE

Executive Summary of the Thesis

Expansion of the coupled solar radiation pressure-J_2 Hamiltonian model to account for the Sun gravitational perturbation and applications

Laurea Magistrale in Space Engineering - Ingegneria Spaziale

Author: Andrea Cecconello

Advisor: Prof. Camilla Colombo

Co-advisor: Andrea Muciaccia

Academic year: 2022-2023

1. Introduction

The Hamiltonian formulation of the perturbed two-body problem has gained popularity due to its ability to describe the effect of conservative perturbation on the orbital dynamics of an object. However, the actual model for low and medium Area-To-Mass ratio (AMR) objects is not able to describe the dynamics induced by the gravitational perturbation of the Sun. This research aims to formulate a new Hamiltonian model of the coupled SRP-Earth oblateness (J_2) and Sun third-body perturbation and assess its potentiality in the field of de-orbiting trajectory design and debris dynamics. For the first application, a new way to exploit the solar radiation pressure and the third-body perturbation to drive the spacecraft towards the Earth is proposed. Additionally, conditions under which low AMR debris may accumulate in asymmetric equilibrium points are computed.

1.1. Fundamentals of SRP-J_2 model

1.1.1 Hypothesis of the model

It is assumed that a spacecraft is affected by a planet gravitational gravity, planetary oblateness, and solar radiation pressure (SRP). In addition, it is assumed that the Sun rays are always perpendicular to the satellite surface (cannonball model), that the influence of planetary albedo is minimal, that the solar flux is constant at 1 AU, and that the satellite is totally in sunlight. Therefore the SRP is modeled as a constant force in the direction of the Earth–Sun line and may be computed from a potential function with these assumptions. The dynamics of the satellite in a geocentric equatorial inertial frame can be modelled by the Hamiltonian:

$$\mathcal{H} = \mathcal{H}_{kep} + \mathcal{H}_{J_2} + \mathcal{H}_{SRP} \tag{1}$$

Assuming that the Keplerian contribute is constant due to the conservative dynamics, that the fast angle of the dynamics is the mean anomaly M, it is possible to integrate in close form the perturbing terms $\mathcal{H}_{J_2}$, $\mathcal{H}_{\text{SRP}}$ with respect to the mean anomaly for a full period of the orbit. The resulting single-averaged Hamiltonian has 2.5 DoFs (two degrees-of-freedom and an explicit time dependence through the ecliptic longitude of the Sun $\lambda_\odot(t) = \lambda_{\odot_0} + n_\odot t$). Assuming a dummy action with the same frequency of the Sun orbit, is possible to reduce the Hamiltonian to an autonomous form with 3 DoFs (Gkolias et al. [1]). Then, it is possible to apply the argument developed in Daquin et al. [2] for lunisolar gravitational perturbations, adapted to the solar radiation pressure effect, under the assumption that only one periodic term j

is relevant at a time for the motion of the small body, and than reduce the Hamiltonian to a 1 DoF system (in resonant variables):

$$\begin{aligned} H_{\psi_j} =& \frac{C_{J_2}\mu^3\left(n_1^4\Psi^2 - 3(\Pi + n_1 n_2 \Psi)^2\right)}{n_1^7 4L^3\Psi^5} + \\ &- \frac{C_{\mathrm{SRP}}}{\mu} L^2 \sqrt{1 - \frac{n_1^2\Psi^2}{L^2}}\mathcal{T}_j \cos\psi \\ &+ n_s(n_3\Psi + K) \end{aligned} \tag{2}$$

where Ψ is the conjugate momentum associate to the eccentricity and ψ is the critical angle defined as:

$$\psi_j = n_1\dot{\omega} + n_2\dot{\Omega} + n_3 n_\odot, \tag{3}$$

where n_1, n_2, n_3, and $\mathcal{T}_j$ depends on the resonance j (see [3]), $C_{J_2} = \mu R_\oplus J_2$, $C_{SRP} = \frac{3}{2}P_\odot c_R \frac{A}{m}$, $L = \sqrt{\mu a}$, K dummy action, and Π is the second integral of motion:

$$\Pi = (-n_2 + n_1\cos(i))\sqrt{\mu a(1-e^2)}, \tag{4}$$

which can be used to label the phase space.

1.1.2 Equilibrium and stability

The equilibrium points of the dynamical system can be computed imposing the gradient of the Hamiltonian to zero (both with respect to the coordinate (Ψ, ψ) or (e, ψ)). The stability of the equilibrium points can be evaluated by computing the eigenvalues of the Hessian matrix evaluated at the equilibrium. If the eigenvalues are complex conjugated, the equilibrium point is stable. If they are positive, the equilibrium point is unstable.

1.1.3 Bifurcation map and contributes to the topic

The bifurcation analysis is the study of changes in topological structure of a given family of curves when a small change in one or more bifurcation parameters happens. For the analysis performed in this work, $i_{e=0}$ (or Π_0) is considered as the first bifurcation parameter and a as the second, keeping the AMR fixed.
For each semimajor-axis, for the AMR considered, and in the range $e \in]0, 1[$, the commensurability equation is solved for both the angular positions of the equilibrium points ($\psi = 0, \pi$). Along the family of curves in the plane (e, Π_0), the Hessian is evaluated at the equilibrium point, and when for a triplet (a, Π_0, e) the eigenvalues product is zero, a bifurcation is found. Then, by converting the value of the second integral of motion to the correspondent inclination $i_{e=0}$ by its definition Equation (4), the coordinates (a, $i_{e=0}$) are plotted on the bifurcation map. The first contribute of this work to the literature regards the bifurcation analysis of the first resonance:

- in the regions (I), (II), and (VI) two new equilibria at very high eccentricity are found, hence the total number of equilibria is higher than those found in literature. Those points comes from the second solution of the commensurability equation;
- a completely new region (labelled (VII) see Figure 1), is found between the regions (III) and (IV) and it characterises the transition across the trans-critical bifurcation which separates the (III) from the (IV).

Table 1: Number of equilibria and their stability (S: stable, U: unstable) for the resonance with argument ψ_1, corresponding to the seven regions identified.

Region	Total	$\psi = 0$	$\psi = \pi$
I	5	1S and 1U	2S and 1U
II	7	2S and 2U	2S and 1U
III	3	1S and 1U	1S
IV	3	1S	1S and 1U
V	1	-	1S
VI	5	1S	2S and 2U
VII	3	2S	1S

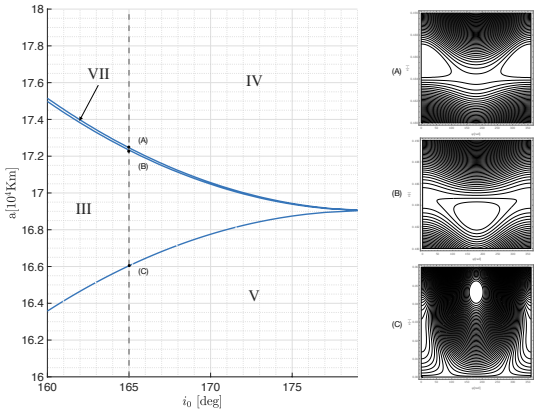

Figure 1: Detail of region (VII) at AMR = 1 m^2/kg.

2. Extended SRP-J_2-Sun model

In this section the main innovation introduced by this work to the literature are reported.

2.1. Previous statements

The innovation introduced by this work is to add the Sun gravity contribute to the state-of-art model and then analyse it using the tool of the bifurcation analysis.
In [1], for the value of (a, e, i) and AMR considered, the contribute of the Hamiltonian of the Sun gravitational perturbation $\mathcal{H}_\odot$ is negligible with respect to that of the SRP following $\mathcal{H}_{SRP}$. Therefore, the following relation holds:

$$\left|\frac{\mathcal{H}_{\odot j}}{\mathcal{H}_{SRPj}}\right| << 1 \tag{5}$$

where j is the resonance considered. However, for some specific ranges of the elements mentioned above the relation is no longer valid, consequently a more complete model has to be considered.

2.2. Hamiltonian formulation

The Hamiltonian function associated to the gravitational perturbation of the Sun gravity is outlined in the following section.

2.2.1 Hypothesis

The hypothesis behind the formulation of the Sun third-body extension of the SRP-J_2 model are the same stated for the SRP-J_2 model in Section 1.1.1. In addition to that:

- the Sun is lying on a circular orbit on the ecliptic plane at 1AU distance from the center of the Earth;
- the precession of the equatorial plane over the ecliptic is neglected, which is known to have a long-term effect, on time scales of decades.

2.2.2 Hamiltonian of the Sun gravity perturbation

The perturbing potential of a third-body on spacecraft close to a central body can be expressed as a power series of the parallactic factor (r/r_{3b}) as reported by Lara et al. [4]. Then, the position of the perturber is written in the Earth's equatorial frame and averaged over the mean anomaly M of the spacecraft. The averaging process results in:

$$\bar{\mathcal{H}}_\odot = -\frac{a^2 n_\odot^2}{64}\sum_{i=0}^{2}\sum_{j=-2i}^{2}\sum_{p=-1}^{1} \mathcal{Y}_i K_{2i,l,2p} \times \cos(2i\omega + l\Omega + 2p\lambda_\odot) \tag{6}$$

Table 2: Sun gravity resonant terms. Coefficient $\mathcal{Y}_i$ and $\mathcal{K}_{2i,l,2p}$ in Equation (6) taken from Lara et. al. [4].

i	l	p	$\mathcal{K}_{2i,j,2p}$	ϕ	j
1	2	-1	$\frac{1}{4}(1+c_\epsilon)^2(1+c_i)^2$	$2\omega + 2\Omega - 2\lambda_\odot$	1
1	-2	1	$\frac{1}{4}(1+c_\epsilon)^2(1-c_i)^2$	$2\omega - 2\Omega + 2\lambda_\odot$	2
2	0	-2	$\frac{3}{2}s_\varepsilon^2 s_i^2$	$2\omega - 2\lambda_\odot$	3
2	0	2	$\frac{3}{2}s_\varepsilon^2 s_i^2$	$2\omega + 2\lambda_\odot$	4
1	1	1	$-\frac{1}{4}(c_\epsilon - 1)^2(c_i + 1)^2$	$2\omega + 2\Omega + 2\lambda_\odot$	5
-1	1	1	$\frac{1}{4}(c_\epsilon - 1)^2(c_i - 1)^2$	$-2\omega + 2\Omega + 2\lambda_\odot$	6

where the coefficients $\mathcal{Y}_i = 30e^2$ (for all the resonances), and $K_{2i,l,2p}$ is reported in Table 2.
Then, only the coefficients $(i,\ j,\ p)$ for which the SRP and Sun gravity Hamiltonian have the same critical angle, are considered. By following the same procedure as for the SRP-J_2 model (see Section 1.1.1), the Hamiltonian model is reduced to a single-resonant model, and since it has the same critical angle as the SRP contribute, it is possible to make the Hamiltonian autonomous by adding a dummy action with frequency $n_\odot$. The distilled Hamiltonian written in Delaunay variables is:

$$\begin{aligned}\bar{\mathcal{H}} = &\frac{\mathcal{C}_{J_2}\mu^3(G^2 - 3H^2)}{4G^5L^3} + \\ &- \frac{\mathcal{C}_{\mathcal{SRP}}\sqrt{1 - G^2/L^2}L^2}{\mu}\sum_{j=1}^{6}\mathcal{T}_j\cos\psi_j + \\ &- \frac{L^4 n_\odot^2}{64\mu^2}\sum_{j=1}^{6}\mathcal{Y}_j K_j \cos 2\psi_j + n_3(n_\odot\Psi + K)\end{aligned} \tag{7}$$

The resulting isolated resonance model has the form of a second Andoyer fundamental model of resonance, in the shape of:

$$\mathcal{K} = \mathcal{A}(\Phi,\Psi) + \mathcal{B}_1(\Phi,\Psi)\cos\phi + \mathcal{B}_2(\Phi,\Psi)\cos 2\phi \tag{8}$$

where, $\mathcal{A}$ is associated with the contribute of the secular J_2, and the $\mathcal{B}_{1,2}$ are associated to the contribute of SRP and Sun gravity.

2.2.3 Equilibrium

The equilibrium are computed imposing null gradient of the Hamiltonian:

$$\begin{aligned}\nabla\mathcal{H}_{\psi,j} &= -\mathcal{B}_{\mathrm{SRP},j}\sin\psi_j - 2\mathcal{B}_{\odot,j}\sin 2\psi_j, \\ \nabla\mathcal{H}_{e,j} &= \frac{\partial\mathcal{H}_{J_2}}{\partial e} + \frac{\partial\mathcal{B}_{\mathrm{SRP},j}}{\partial e}\cos\psi_j + \\ &\quad + \frac{\partial\mathcal{B}_{\odot,j}}{\partial e}\cos 2\psi_j + n_3 n_\odot\frac{\partial\Psi}{\partial e}.\end{aligned} \tag{9}$$

From the equation of $\nabla\mathcal{H}_{\psi,j}$ the critical angles are at $\psi = 0, \pi$ (here called *symmetric* equilibrium

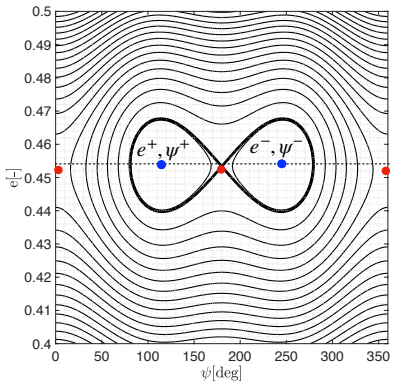

Figure 2: Phase space of the extended SRP-J_2-Sun model relative to the first resonance at $a = 12000$ km, $i_{e=0} = 19.5°$ and AMR $= 0.1\ m^2/\text{kg}$.

points), and at intermediate value (from here called *asymmetric* equilibrium points).
The former are located at $\psi = \pi, 0$, the latter instead, simplifying by $\sin(\psi) \neq 0$ the $\nabla\mathcal{H}_{\psi,j}$, are located at:

$$\cos\psi = -\frac{\mathcal{B}_{\text{SRP}_j}}{4\mathcal{B}_{\odot,j}},. \tag{10}$$

They are represented in Figure 2 with blue dots.

2.2.4 Dynamical regimes

The dynamics is strongly influenced by the AMR; hence, the dynamics is classified according to the AMR of the object. For this scope a new parameter $\sigma^*_{i,j}$ is defined, and used to identify as the critical value $\sigma_{i,j}$ of AMR such that, under certain circumstances defined below, the dynamical model collapse to the coupled SRP, J_2 model. Re-writing the Equation (10), it is defined as:

$$\sigma^*_{i,j} = \frac{15}{8}\frac{\mathcal{K}_j}{\mathcal{T}_j}\frac{n_\odot^2}{P_\odot c_R} a e^{eq}_{i,j} \tag{11}$$

where the i-th equilibrium and j-th resonance are considered. The just derived condition constitutes the generation of a peculiar kind of **bifurcation** which has not yet described in literature. Hence the dynamical regimes stated before, from here, are defined as:

- first dynamical regime for AMR $= 0$;
- second dynamical regime for $0 <$ AMR $< \sigma^*_{i,j}$;
- third dynamical regime for AMR $\geq \sigma^*_{i,j}$ (see Section 1.1.1).

2.2.5 Dynamical structure for AMR $= 0$, resonance $j = 1$

If it is assumed that the spacecraft has negligible area, the dynamics can be described by the coupled Sun gravity and Earth oblateness model. If it is consider the second equation of Equation (9), with $C_{\text{SRP}} = 0$ it is immediate to see that the equilibrium points are at critical angles $\psi_{\odot,J_2} = 0, \frac{\pi}{2}, \pi, \frac{3\pi}{2}$ and π. The bifurcation analysis for AMR $= 0$ is done following similar procedure as the one performed for the SRP-J_2 model. The two regions identified (see Figure 3: the first at the left of the black line, and the second at its right) are described in table 3.

Table 3: Number of equilibria and their stability (S: stable, U: unstable) for the resonance with argument ψ_1.

Region	Total	$\psi = 0$	$\psi = \pi/2$	$\psi = \pi$
(A)	9	2 U, 1S	1 U, 2 S	2 U, 1S
(B)	3	1 U	1 S	1 U

2.2.6 Dynamical structure for $0 < AMR < \sigma^*$, resonance $j = 1$

The Hamiltonian analysed is the one presented in Equation (7) but specialised with the resonance terms of the first resonance. The bifurcation analysis of this dynamics for the symmetric equilibrium points is the same as for the SRP-J_2 model.
The angular position of the asymmetric equilibrium points arising from $\psi = \pi/2$ moves towards $\psi = \pi$ for increasing AMR; when they reach $\psi = \pi$ a bifurcation occurs.
In detail, for each a, $e \in]0, 1[$, and resonant inclination (computed solving the commensurability equation at AMR $= 0$, $\psi = \pi/2$, since the eccentricity of the asymmetric point at AMR $= 0$ is the same up to $\sigma^*_{i,j}$), the $\sigma^*_{i,j}$ is computed from Equation (11) and compared with AMR of the object. If the bifurcation condition is verified, the corresponding coordinates are reported in the (a, $i_{e=0}$) diagram. Since the equilibrium points for a value of $i_{e=0}$ are at maximum three, it follows that three more bifurcation lines appear in the bifurcation map. In particular, in Figure 3, with yellow lines are indicated the two branches of the bifurcations associated with the first two equilibria, and with green, those associated with the third equilibrium.
For the regions intersected by the *asymmetric* bifurcation, above those lines, an asymmetric equilibrium is added as reported in Figure 3.

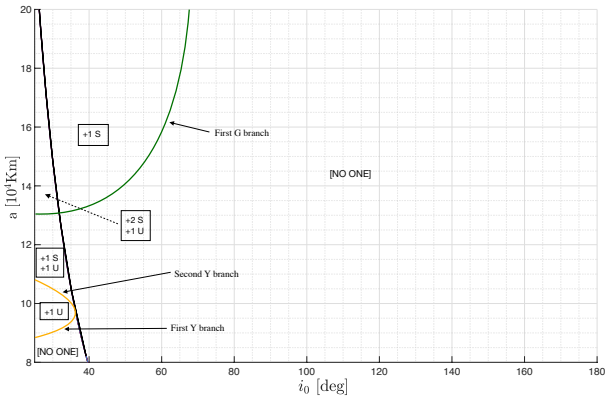

Figure 3: Bifurcation analysis plot for the $\odot, J_2$ model with i_0 from 0 [deg] to 180 [deg], a from 8000 km to 30000 km and $j = 1$. Bifurcation at $i_0 = 29.0085°$ for $a = 16000$ km.

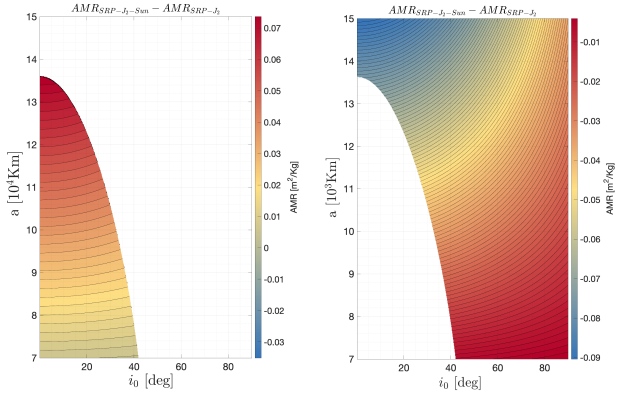

Figure 4: Comparison between the AMR required to deorbit near $\psi = \pi$ (left) and $\psi = 0$ (right).

3. Application to de-orbiting design and debris analysis

Using the techniques of dynamical system theory, this chapter extracts relevant information for de-orbiting design and debris dynamics analysis.

3.0.1 De-orbit from a circular inclined orbit

Similar to what was done in the literature regarding the de-orbit from a circular inclined orbit, it is shown how de-orbiting may occur within the extended SRP-J_2-Sun model. Given that the semimajor-axis, the Hamiltonian function and the second integral of motion Π are conserved, it is possible to solve a two-point boundary value problem for the minimum value of AMR connecting the initial and the final conditions. The initial condition is a circular inclined orbit, while, the final is an orbit with $e_{cr} = 1 - R_\oplus/a$. The final angular configuration corresponds to the maximum eccentricity increase, which, in the extended model, can be found on an asymmetric equilibrium points. The procedure is described in the following paragraph. For each $a \in [7500, 15000]$ km and $i_{e=0} \in [0°, 90°]$ the following equation has been solved for $\psi_{j,cr} = 0$:

$$\mathcal{H}_j(0, \psi_{j,1}; \Pi, L, \mathcal{C}_{\text{SRP}}) = \mathcal{H}_j(e_{cr}, \psi_{j,cr}; \Pi, L, \mathcal{C}_{\text{SRP}}). \tag{12}$$

If the value of $\mathcal{C}_{\text{SRP}} > 0$, the de-orbit happens in $\psi_{j,cr} = 0$, otherwise it may happen in the range $\psi \in]\pi/2, \pi]$. Therefore, the equation is solved again taking into account that for the asymmetric equilibrium point the angular configuration and AMR are dependent (see Equation (10)). Then, using the just computed AMR, the de-orbiting angular configuration is checked evaluating Equation (10); if $\cos(\psi) \in]-1; 0[$, the de-orbit happens in an asymmetric points, otherwise, if $\cos(\psi) \leq -1$, it happens in $\psi = \pi$. In Figure 4, are reported the comparison between the state-of-art model and the extended, for de-orbiting at $\psi = 0$ and $\psi \in]\pi/2, \pi]$, respectively. Using this strategy near a bifurcation or for $\psi_{cr} = 0$, the AMR is less than the one computed in literature, because it exploits also the Sun gravity.

3.0.2 De-orbit from unstable point

This strategy exploits a spacecraft initially located at a unstable point for the extended dynamics at $\psi = \pi$. The algorithm developed evaluates for (a, $i_{e=0}$, $\psi_1 = \pi$, AMR $= 0$) if, exploiting the double-lobe phase space, is possible to reach the critical eccentricity at $\psi = \pi/2$. If it is true, it solves Equation (12) considering:

- $e_0 = e(\psi = \pi, \text{AMR} = 0)$ (initial guess);
- $\cos(\psi_{cr})$ from Equation (10);
- initial and final inclination corresponding to the initial and final eccentricity computed through the conservation of Π;

The unknowns are AMR and the eccentricity of the initial unstable point, since it depends on the AMR. The first unknown is full-filled with Equation (10), the second instead is computed through an iterative algorithm which after each iteration computes the eccentricity at the initial point with a new AMR, solving:

$$\kappa_1 \mathcal{C}_{\text{SRP}}^2 + \kappa_2 \mathcal{C}_{\text{SRP}} + \kappa_3 = 0. \tag{13}$$

Where the coefficients depend on physical parameters ($\mu, n_\odot, J_2$, ecc.), initial and, final conditions. This equation is derived from Equation (12) at which as final angular condition is imposed the asymmetrical equilibrium point Equation (10).
In Figure 5 is reported the de-orbiting map in the

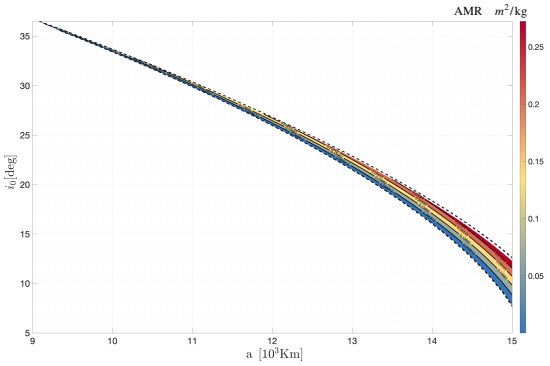

Figure 5: Maximum AMR for deorbit from a given a and inclination of initially circular orbit i_0

range of $a \in [9000, 15000]$ km. The black dashed lines represent the upper and lower border of the feasible region, and the contour lines the **maximum** AMR which allows the re-entry. In fact, if the AMR is inferior to this limit, the width of the double-lobe is inferior, hence, the de-orbiting is not guaranteed.
The newly presented technique utilizes the previously described notion. In detail, the solar sail remains open throughout the duration of the mission, and closes to ensure the de-orbiting. Unfortunately, from a practical standpoint it is now fairly impractical. This because the maneuver can only be used if the spacecraft is originally positioned near its orbit critical eccentricity.

3.1. Application to debris dynamics

The condition under which low AMR debris are trapped into the asymmetric equilibra, are derived in this work.
For a synthetic population generated from the standard NASA breakup model, a spacecraft is virtually exploded near a stable asymmetric point located at $a = 13000$ km, $i_{e=0} = 19°$ and AMR $= 0.1\ m^2/\text{kg}$. The population is propagated for 100 years using a full-dynamics semi-analytical propagator, and those debris (having AMR $< \sigma^*_{i,j}$) which remains nearby the initial condition are compared with the phase space described by their mean (a, i, AMR). The populations are propagated starting from $\psi = 0, \pi$ (unstable points) and $\psi = \pi/2$ (stable point). Some debris generated from a stable region remain trapped in it, instead, those debris that are generated starting from an unstable points, do not accumulate in a specific region.

4. Conclusions

An Hamiltonian model has been derived to represent the complex dynamics of low and medium AMR objects subject to SRP-J_2-Sun gravity perturbations. The new phase space shape was exploited for passive de-orbiting of dead spacecrafts, and in some cases the minimum AMR computed is lower than literature. It is possible to derive the conditions under which low/medium AMR debris accumulates in space, such as objects with an AMR lower than a "discriminant" AMR.

5. Acknowledgements

I would like to express my sincere gratitude to my supervisor professor Camilla Colombo and co-supervisor Andrea Muciaccia, for their assistance at every stage of this research project an for her insightful comments and suggestions that made this thesis work scientifically valuable.

References

[1] Ioannis Gkolias, Elisa Maria Alessi, and Camilla Colombo. “Dynamical taxonomy of the coupled solar radiation pressure and oblateness problem and analytical deorbiting configurations”. In: *Celestial Mechanics and Dynamical Astronomy* 132 (11-12 Dec. 2020). ISSN: 15729478. DOI: 10.1007/s10569-020-09992-2.

[2] Jerome Daquin et al. “The dynamical structure of the MEO region: long-term stability, chaos, and transport”. In: *Celestial Mechanics and Dynamical Astronomy* 124 (Apr. 2016). DOI: 10.1007/s10569-015-9665-9.

[3] Elisa Maria Alessi, Camilla Colombo, and Alessandro Rossi. “Phase space description of the dynamics due to the coupled effect of the planetary oblateness and the solar radiation pressure perturbations”. In: *Celestial Mechanics and Dynamical Astronomy* 131 (Sept. 2019). DOI: 10.1007/s10569-019-9919-z.

[4] Martin Lara et al. “Long-term evolution of Galileo operational orbits by canonical perturbation theory”. In: *Acta Astronautica* 94 (2 2014), pp. 646–655. ISSN: 00945765. DOI: 10.1016/j.actaastro.2013.09.008.